CHEMISTRY OF MATERIALS

Article

pubs.acs.org/cm

Low Turn-on Voltage, High-Power-Efficiency, Solution-Processed Deep-Blue Organic Light-Emitting Diodes Based on Starburst Oligofluorenes with Diphenylamine End-Capper to Enhance the HOMO Level

Cui Liu,[†,§] Qiang Fu,[‡,§] Yang Zou,[†] Chuluo Yang,*[,†] Dongge Ma,*[,‡] and Jingui Qin[†]

[†]Hubei Collaborative Innovation Center for Advanced Organic Chemical Materials, Hubei Key Lab on Organic and Polymeric Optoelectronic Materials, Department of Chemistry, Wuhan University, Wuhan 430072, People's Republic of China

[‡]State Key Laboratory of Polymer Physics and Chemistry, Changchun Institute of Applied Chemistry, Chinese Academy of Sciences, Changchun 130022, People's Republic of China

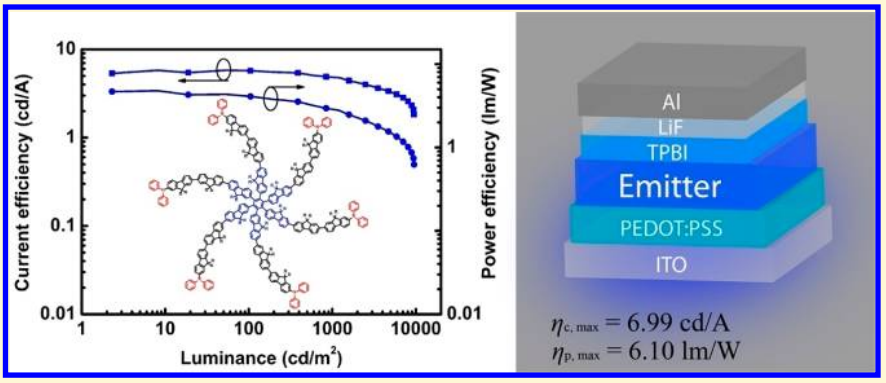

ABSTRACT: Two new star-shaped oligofluorenes, **HFB-diF-Dpa** and **HFB-terF-Dpa**, with a hexakis(fluoren-2-yl)benzene core and six diphenylamine end-cappers were designed and synthesized. The peripheral diphenylamine groups enhance the HOMO energy levels of the materials, and the bulky star-shaped structures efficiently suppress the intermolecular interaction. Their thermal, photophysical, and electrochemical properties were investigated. The two compounds display strong deep-blue emission both in solution and solid state. Solution-processed devices based on these starbursts exhibit highly efficient and stable deep-blue electroluminescence. Their high-lying HOMO energy levels match very well with that of the hole-injecting material. The double-layered device featuring **HFB-diF-Dpa** as emitter shows a low turn-on voltage of 3.6 V, a maximum current efficiency of 6.99 cd A^{-1}, and a maximum external quantum efficiency of 5.45% with the CIE coordinate of (0.154, 0.136). In particular, the combination of low driving voltage and high EQE provides an outstanding maximum power efficiency of 6.10 lm W^{-1}, which is the highest for nondoped deep-blue OLEDs based on solution-processable materials. Moreover, these devices present small values of efficiency roll-off at high brightness up to 1000 cd m^{-2}.

INTRODUCTION

Organic light-emitting diodes (OLEDs) have attracted considerable scientific and industrial attention because of their applications in flat-panel displays and solid-state lighting resources.[1−13] Full-color displays require primary RGB emission of relatively equal stability, efficiency, and color purity. The development of deep-blue emission, which is defined as having blue electroluminescence (EL) emission with a Commission Internationale de l'Eclairage (CIE) *y*-coordinate value of less than 0.15, is of special significance because such emitters can not only effectively reduce the power consumption of a full-color OLED but also be utilized to generate light of other colors by energy cascade to a lower-energy fluorescent or phosphorescent dopant.[14−16] However, the intrinsic wide band gap essential for blue emission often results in low electron affinities of these blue-light-emitting materials. This hampers charge injection and balances, consequently impairing the efficiency of blue OLEDs.

Polyfluorene and its derivatives are considered to be the most promising blue emitting materials[17−19] due to their high photoluminescence (PL) efficiencies, wide band-gaps, good thermal stabilities, interesting morphological properties, and easy tunability of properties by substitution and/or copolymerization.[20−25] However, the application of polyfluorenes as blue emitters in OLEDs is hampered by their undesirable long-wavelength emission in the process of photoirradiation, heat treatment, or device operation, which has been attributed to physical[26−30] or chemical[31,32] degradation processes. Recently,

Received: November 30, 2013
Revised: April 27, 2014
Published: April 27, 2014

   dx.doi.org/10.1021/cm4039522 | *Chem. Mater.* 2014, 26, 3074−3083

monodisperse oligofluorenes that can be deposited via solution process have been of great interest for use in OLEDs.[33−42] In comparison with polymers, monodisperse oligofluorenes are characterized by well-defined and uniform molecular structures as well as high chemical purity. It has been demonstrated that the performance and stability of monodisperse oligofluorenes in OLEDs are superior to those of polyfluorenes.[43−45] Several series of star-shaped oligofluorenes with various cores such as benzene,[46] triazatruxene,[34] pyrene,[37] 4,4′,4″-tris(carbazol-9-yl)-triphenylamine (TCTA),[35] 1,3,5-tri(anthracen-10-yl)benzene,[39] fully bridged triphenylamine,[40] truxene,[47] and spirofluorene[33] have been reported.

In our previous work, we have reported a series of six-arm star-shaped oligofluorenes with a hexakis(fluoren-2-yl)benzene core.[42] These oligomers exhibit good solubility, efficient deep-blue emission, and good film-forming ability. The devices based on these materials achieved good performances and striking deep-blue EL color stability. However, the highest occupied molecular orbital (HOMO) energy levels of these materials are very low, resulting in a very high turn-on voltage, and then low luminance and power efficiency. To address this issue, herein we designed and synthesized two new star-shaped oligofluorenes **HFB-diF-Dpa** and **HFB-terF-Dpa** by introducing a diphenylamine group in each fluorene arm to enhance the HOMO energy level of the materials. The thermal, photophysical, and electrochemical properties of **HFB-diF-Dpa** and **HFB-terF-Dpa** as well as the characteristics of devices incorporating these materials were investigated. All these compounds show deep-blue emission with high fluorescence quantum yields in film. Their high-lying HOMO energy levels match very well with that of the hole-injecting material. Solution-processed devices based on these starbursts exhibit efficient deep-blue electroluminescence and achieve a maximum current efficiency of 6.99 cd A^{-1}, and a maximum power efficiency of 6.10 lm W^{-1}, with the CIE coordinate of (0.154, 0.136), which is among the highest for nondoped deep-blue OLEDs based on solution-processed materials.

EXPERIMENTAL SECTION

General Information. ^{1}H NMR and ^{13}C NMR spectra were measured on a MECUYR-VX300 spectrometer. Elemental analyses of carbon, hydrogen, and nitrogen were performed on a Vario EL III microanalyzer. Mass spectra were measured on a ZAB 3F-HF mass spectrophotometer. Matrix-assisted laser-desorption/ionization time-of-flight (MALDI-TOF) mass spectra were performed on Bruker BIFLEX III TOF mass spectrometer. UV−vis absorption spectra were recorded on a Shimadzu UV-2500 recording spectrophotometer. Photoluminescence (PL) spectra were recorded on a Hitachi F-4500 fluorescence spectrophotometer. The PL quantum yields of solid state films were measured by an absolute method using the Edinburgh Instruments (FLS920) integrating sphere excited with Xe lamp. Differential scanning calorimetry (DSC) was performed on a NETZSCH DSC 200 PC unit at a heating rate of 10 °C min^{-1} from room temperature to 300 °C under argon. The glass transition temperature was determined from the second heating scan. Thermogravimetric analysis (TGA) was undertaken with a NETZSCH STA 449C instrument. The thermal stability of the samples under a nitrogen atmosphere was determined by measuring their weight loss while heating at a rate of 15 °C min^{-1} from 25 to 800 °C. Cyclic voltammetry was carried out in nitrogen-purged THF (reduction scan) and dichloromethane (oxidation scan), respectively, with a CHI voltammetric analyzer. Tetrabutylammonium hexafluorophosphate (TBAPF6) (0.1 M) was used as the supporting electrolyte. The conventional three-electrode configuration consists of a platinum working electrode, a platinum wire auxiliary electrode, and an Ag wire pseudoreference electrode with ferrocenium−ferrocene (Fc^+/Fc) as the internal standard. Cyclic voltammograms were obtained at a scan rate of 100 mV s^{-1}. Formal potentials are calculated as the average of cyclic voltammetric anodic and cathodic peaks. The onset potential was determined from half-wave potential of the oxidation.

Device Fabrication and Measurement. The two types of hole-injection material poly(3,4-ethylenedioxythiopene):poly-(styrenesulfonate) (PEDOT:PSS) and electron-transporting material TPBI were commercially available. Commercial ITO coated glass with sheet resistance of 10 Ω $square^{-1}$ was used as the starting substrates. Before device fabrication, the ITO glass substrates were precleaned carefully and treated by oxygen plasma for 2 min. PEDOT:PSS was spin-coated to smooth the ITO surface and promote hole injection, and then the emissive layer was spin-coated from chlorobenzene solution. The samples were annealed at 120 °C for 30 min to remove residual solvent. The thickness of the EML was about 50 nm. Finally, an electron-transporting layer of 1,3,5-tris(*N*-phenylbenzimidazol-2-yl)benzene (TPBI, 30 nm) and a cathode composed of lithium fluoride (LiF, 1 nm) and aluminum (Al, 100 nm) were sequentially deposited onto the substrate by vacuum deposition in the vacuum of 10^{-6} Torr. The current density−voltage−brightness (*J*−*V*−*L*) of the devices was measured with a Keithley 2400 Source meter and a Keithley 2000 Source multimeter equipped with a calibrated silicon photodiode. The electroluminiscence (EL) spectra were measured by JY SPEX CCD3000 spectrometer. The EQE values were calculated according to previously reported methods.[48] All measurements were carried out at room temperature under ambient conditions.

Synthesis. (9,9-Dihexyl-7-(4,4,5,5-tetramethyl-1,3,2-dioxaborolan-2-yl)-9*H*-fluoren-2-yl)(trimethyl)silane (**F1**) and (7′-bromo-9,9,9′,9′-tetrahexyl-9*H*,9′*H*-2,2′-bifluoren-7-yl)(trimethyl)silane (**F2**) were prepared following the reported procedures.[49] 2,2′-Ethyne-1,2-diylbis(7-bromo-9,9-dihexyl-9*H*-fluorene) (**A0**) was synthesized according to our previous method.[42]

*7-Bromo-9,9,9′,9′-tetrahexyl-7′-iodo-9H,9′H-2,2′-bifluorene (**F3**).* To a solution of **F2** (3.11 g, 3.80 mmol) in anhydrous CH_2Cl_2 (40 mL), ICl (0.63 M in CH_2Cl_2, 6.0 mL, 3.80 mmol) was added dropwise at 0 °C. After stirring for 30 min at 0 °C, the reaction mixture was poured into a $Na_2S_2O_3$ aqueous solution with vigorous stirring until discoloration for extraction with CH_2Cl_2. The organic layer was washed with brine for several times and dried over anhydrous Na_2SO_4. The extract was evaporated to dryness, and the residue was purified by column chromatography on silica gel using petroleum ether as the eluent to give a white solid (3.26 g). Yield: 98%. ^{1}H NMR (300 MHz, $CDCl_3$, δ): 7.76 (d, *J* = 8.1 Hz, 2H), 7.71−7.52 (m, 7H), 7.50−7.43 (m, 3H), 2.10−1.88 (m, 8H), 1.19−0.99 (m, 24H), 0.77 (t, *J* = 6.9 Hz, 12H) 0.73−0.61 (m, 8H). ^{13}C NMR (75 MHz, $CDCl_3$, δ): 153.68, 153.51, 151.40, 151.18, 141.23, 141.06, 140.65, 140.02, 139.64, 136.18, 132.40, 130.29, 126.53, 121.71, 121.35, 120.31, 92.78, 55.71, 55.79, 40.49, 31.69, 29.85, 23.98, 22.80, 14.25. MS (EI) *m*/*z*: 870.21. Anal. Calcd for $C_{50}H_{64}BrI$: C 68.88, H 7.40. Found: C 68.58, H 7.13.

*(7″-Bromo-9,9,9′,9′,9″,9″-hexahexyl-9H,9′H,9″H-2,2′:7′,2″-terfluoren-7-yl)(trimethyl)silane (**F4**).* To a mixture of **F1** (1.86 g, 3.50 mmol), **F3** (3.05 g, 3.50 mmol), $Pd(PPh_3)_4$ (0.058 g, 0.05 mmol), and 2 M K_2CO_3 (9.00 mL, 18.00 mmol) was added degassed toluene (40 mL). The solution was heated to 100 °C and stirred at this temperature for 48 h under argon. After cooling to room temperature, the solution was extracted with CH_2Cl_2 and the organic layer was washed with brine and water, and then dried over anhydrous Na_2SO_4. After the solvent had been removed, the residue was purified by column chromatography on silica gel using petroleum ether as the eluent to give a white solid (3.10 g). Yield: 77%. ^{1}H NMR (300 MHz, $CDCl_3$, δ): 7.84−7.70 (m, 6H), 7.70−7.57 (m, 8H), 7.57−7.44 (m, 4H), 2.18−1.92 (m, 12H), 1.19−1.00 (m, 36H), 0.90−0.62 (m, 30H), 0.33 (s, 9H). ^{13}C NMR (75 MHz, $CDCl_3$, δ): 153.42, 151.89, 151.27, 150.34, 141.57, 141.19, 140.77, 140.47, 140.33, 140.03, 139.38, 139.16, 132.04, 130.19, 128.96, 127.81, 127.38, 126.44, 126.35, 126.21, 121.67, 121.27, 121.17, 120.20, 119.20, 55.71, 55.50, 55.29, 40.53, 40.33, 31.67, 31.57, 29.85, 23.92, 22.78, 22.73, 14.25, −0.62. MALDI-TOF *m*/*z*: 1151.7. Anal. Calcd for $C_{78}H_{105}BrSi$: C 81.42, H 9.20. Found: C 81.62, H 9.49.

dx.doi.org/10.1021/cm4039522 | *Chem. Mater.* 2014, 26, 3074−3083

*7-Bromo-9,9,9′,9′,9″,9″-hexahexyl-7″-iodo-9H,9′H,9″H-2,2′:7′,2″-terfluorene (**F5**).* **F5** was prepared according to the same procedure as **F3** but using compound **F4** to give a white solid. Yield: 96%. ^{1}H NMR (300 MHz, $CDCl_3$, δ): 7.83 (d, J = 7.5 Hz, 2H), 7.77 (d, J = 8.1 Hz, 2H), 7.72−7.58 (m, 10H), 7.52−7.45 (m, 4H), 2.18−1.89 (m, 12H), 1.22−1.01 (m, 36H), 0.91−0.61 (m, 30H). ^{13}C NMR (75 MHz, $CDCl_3$, δ): 153.62, 153.42, 151.99, 151.28, 151.08, 141.34, 141.15, 140.63, 140.52, 140.25, 140.00, 139.47, 136.07, 132.26, 130.18, 127.39, 126.44, 126.37, 121.66, 121.28, 121.20, 120.23, 92.70, 55.72, 55.65, 55.52, 40.51, 31.66, 29.84, 23.93, 22.78, 14.25. MALDI-TOF m/z: 1202.8. Anal. Calcd for $C_{75}H_{96}BrI$: C 74.79, H 8.03. Found: C 74.96, H 8.19.

*(7′-Bromo-9,9,9′,9′-tetrahexyl-9H,9′H-2,2′-bifluoren-7-yl)-diphenylamine (**F6**).* To a mixture of **F3** (10.90 g, 12.50 mmol), diphenylamine (1.69 g, 10.00 mmol), CuI (0.095 g, 0.50 mmol), sodium *tert*-butoxide (1.44 g, 15.00 mmol), and *trans*-1,2-diaminocyclohexane (0.23 g, 2.00 mmol) was added degassed 1,4-dioxane (40 mL).The solution was heated to 110 °C and stirred at this temperature for 18 h under argon. After cooling to room temperature, the reaction mixture was poured into 150 mL of brine. The solution was extracted with CH_2Cl_2, and the organic layer was washed with brine and water and then dried over anhydrous Na_2SO_4. After the solvent had been removed, the residue was purified by column chromatography on silica gel using petroleum ether/dichloromethane (50:1 by vol) as the eluent to give a white solid (7.85 g). Yield: 86%. ^{1}H NMR (300 MHz, $CDCl_3$, δ): 7.76−7.53 (m, 8H), 7.53−7.44 (m, 2H), 7.31−7.21 (m, 4H), 7.21−7.10 (m, 5H), 7.10−6.98 (m, 3H), 2.03−1.92 (m, 8H), 1.22−1.00 (m, 24H), 0.91−0.62 (m, 20H). ^{13}C NMR (75 MHz, $CDCl_3$, δ): 153.51, 152.69, 151.73, 151.38, 148.30, 147.45, 141.31, 140.60, 140.16, 139.78, 139.36, 136.21, 130.26, 129.47, 129.03, 127.38, 126.48, 124.09, 123.87, 122.78, 121.60, 121.32, 120.72, 120.28, 119.70, 55.79, 55.46, 40.57, 31.77, 29.90, 24.01, 22.83, 14.33. MS (EI) m/z: 911.28. Anal. Calcd for $C_{62}H_{74}BrN$: C 81.55, H 8.17, N 1.53. Found: C 81.73, H 8.25, N 1.67.

*(7″-Bromo-9,9,9′,9′,9″,9″-hexahexyl-9H,9′H,9″H-2,2′:7′,2″-terfluoren-7-yl)diphenylamine (**F7**).* **F7** was prepared according to the same procedure as **F6** but using compound **F5** to give a yellow solid. Yield: 88%. ^{1}H NMR (300 MHz, $CDCl_3$, δ): 7.83−7.73 (m, 4H), 7.73−7.56 (m, 10H), 7.51−7.45 (m, 2H), 7.30−7.21 (m, 4H), 7.17−7.11 (m, 5H), 7.08−6.98 (m, 3H), 2.09−1.82 (m, 12H), 1.22−1.01 (m, 36H), 0.90−0.62 (m, 30H). ^{13}C NMR (75 MHz, $CDCl_3$, δ): 153.44, 152.61, 151.99, 151.62, 151.30, 148.20, 147.31, 141.22, 140.79, 140.41, 140.22, 140.03, 139.89, 139.41, 136.21, 130.22, 129.39, 126.47, 126.37, 126.31, 124.22, 124.01, 123.81, 122.69, 121.65, 121.61, 121.42, 121.30, 121.21, 120.66, 120.23, 119.63, 55.74, 55.54, 55.39, 40.56, 31.74, 31.70, 29.88, 24.05, 22.81, 14.66, 14.32. MALDI-TOF m/z: 1246.7. Anal. Calcd for $C_{87}H_{106}BrN$: C 83.88, H 8.58, N 1.12. Found: C 83.81, H 8.44, N 1.16.

*(9,9,9′,9′-Tetrahexyl-7′-(4,4,5,5-tetramethyl-1,3,2-dioxaborolan-2-yl)-9H,9′H-2,2′-bifluoren-7-yl)diphenylamine (**F8**).* To a mixture of **F6** (4.83 g, 5.29 mmol), bis(pinacolato)diborane (1.61 g, 6.35 mmol), and KOAc (3.14 g, 32 mmol), degassed 1,4-dioxane (25 mL) was added under a flow of argon. Afterward, Pd(dppf)Cl_2 (0.12 g, 0.16 mmol) was added. The solution was heated to 85 °C and stirring at this temperature for 8 h under argon. After cooling to room temperature, the reaction mixture was poured into ice water. The solution was extracted with CH_2Cl_2, and the organic layer was washed with brine and water and then dried over anhydrous Na_2SO_4. After the solvent had been removed, the residue was purified by column chromatography on silica gel using petroleum ether/dichloromethane (2:1 by vol) as the eluent to give a white solid (3.73 g). Yield: 73%. ^{1}H NMR (300 MHz, $CDCl_3$, δ): 7.85−7.70 (m, 4H), 7.70−7.55 (m, 6H), 7.29−7.22 (m, 4H), 7.17−7.11 (m, 5H), 7.07−6.98 (m, 3H), 2.07−1.82 (m, 8H), 1.40 (s, 12H), 1.20−1.00 (m, 24H), 0.82−0.62 (m, 20H). ^{13}C NMR (75 MHz, $CDCl_3$, δ): 152.47, 152.11, 151.45, 150.22, 148.04, 147.13, 143.91, 141.05, 140.24, 140.06, 139.74, 136.04, 133.85, 129.23, 128.92, 127.23, 126.14, 126.01, 123.84, 123.64, 122.52, 121.43, 121.32, 120.46, 120.40, 119.47, 119.40, 119.09, 83.79, 55.30, 55.23, 40.32, 40.14, 40.05, 31.58, 31.54, 31.35, 31.22, 29.71, 29.55, 29.46, 25.04, 24.85, 24.82, 24.71, 23.87, 23.76, 23.64, 23.49, 22.66, 22.49, 22.32, 14.15. MS (EI) m/z: 959.32. Anal. Calcd for $C_{68}H_{86}BNO_2$: C 85.06, H 9.03, N 1.46. Found: C 85.07, H 9.08, N 1.49.

*(9,9,9′,9′,9″,9″-Hexahexyl-7″-(4,4,5,5-tetramethyl-1,3,2-dioxaborolan-2-yl)-9H,9′H,9″H-2,2′:7′,2″-terfluoren-7-yl)diphenylamine (**F9**).* **F9** was prepared according to the same procedure as **F8** but using compound **F7** to give a light yellow solid. Yield: 50%. ^{1}H NMR (300 MHz, $CDCl_3$, δ): 7.87−7.72 (m, 6H), 7.72−7.56 (m, 10H), 7.29−7.20 (m, 4H), 7.17−7.09 (m, 5H), 7.07−6.98 (m, 3H), 2.18−1.82 (m, 12H), 1.40 (s, 12H), 1.22−0.99 (m, 36H), 0.90−0.61 (m, 30H). ^{13}C NMR (75 MHz, $CDCl_3$, δ): 152.60, 152.27, 151.96, 151.60, 150.38, 148.19, 147.28, 144.03, 141.21, 140.70, 140.63, 140.35, 140.07, 139.91, 136.21, 134.05, 129.38, 129.10, 126.27, 123.99, 123.80, 122.68, 121.71, 121.55, 121.42, 120.61, 120.18, 119.62, 119.27, 83.91, 55.51, 55.46, 55.39, 40.57, 40.49, 31.73, 31.68, 29.88, 25.18, 24.03, 22.80, 14.30. MALDI-TOF m/z: 1292.9. Anal. Calcd for $C_{93}H_{118}BNO_2$: C 86.40, H 9.20, N 1.08. Found: C 86.66, H 9.31, N 1.12.

*7″,7‴″-(Ethyne-1,2-diyl)bis(9,9,9′,9′,9″,9″-hexahexyl-N,N-diphenyl-9H,9′H,9″H-(2,2′:7′,2″-terfluoren)-7-amine) (**A1**).* To a mixture of **A0** (0.34 g, 0.40 mmol), **F8** (1,23 g, 1.27 mmol), Pd(PPh_3)$_4$ (0.028 g, 0.024 mmol), and 2 M K_2CO_3 (2.00 mL, 4.00 mmol) was added degassed toluene (10 mL) and ethanol (2 mL). The solution was heated to 100 °C and stirred at this temperature for 48 h under argon. After cooling to room temperature, the solution was extracted with CH_2Cl_2, and the organic layer was washed with brine and water and then dried over anhydrous Na_2SO_4. After the solvent was removed, the residue was purified by column chromatography on silica gel using petroleum ether/dichloromethane (5:1 by vol) as the eluent to give a yellow solid (0.67 g). Yield: 71%. ^{1}H NMR (300 MHz, $CDCl_3$, δ): 7.85−7.78 (m, 5H), 7.78−7.72 (m, 2H), 7.72−7.61 (m, 16H), 7.61−7.57 (m, 7H), 7.31−7.22 (m, 8H), 7.18−7.11 (m, 10H), 7.08−6.98 (m, 8H), 2.17−1.82 (m, 24H), 1.21−0.98 (m, 72H), 0.90−0.62 (m, 60H). ^{13}C NMR (75 MHz, $CDCl_3$, δ): 152.60, 151.98, 151.60, 151.28, 148.18, 147.28, 141.26, 141.18, 140.75, 140.45, 140.35, 140.02, 139.85, 136.18, 129.36, 126.42, 126.35, 126.26, 126.15, 123.99, 123.79, 122.66, 121.71, 121.66, 121.58, 121.42, 120.61, 120.47, 120.18, 119.95, 119.64, 119.56, 90.91, 55.52, 55.38, 40.70, 40.57, 40.49, 31.74, 31.67, 29.95, 29.87, 24.03, 22.84, 22.79, 14.28. MALDI-TOF m/z: 2356.3. Anal. Calcd for $C_{176}H_{212}N_2$: C 89.74, H 9.07, N 1.19. Found: C 89.48, H 9.27, N 1.23.

*7‴,7⁗″-(Ethyne-1,2-diyl)bis(9,9,9′,9′,9″,9″,9‴,9‴-octahexyl-N,N-diphenyl-9H,9′H,9″H,9‴H-(2,2′:7′,2″:7″,2‴-quaterfluoren)-7-amine) (**A2**).* **A2** was prepared according to the same procedure as **A1** but using compounds **A0** and **F9** to give a yellow solid. Yield: 56%. ^{1}H NMR (300 MHz, $CDCl_3$, δ): 7.87−7.76 (m, 12H), 7.76−7.57 (m, 30H), 7.31−7.22 (m, 8H), 7.18−7.11 (m, 10H), 7.08−6.97 (m, 8H), 2.19−1.81 (m, 32H), 1.21−0.95 (m, 96H), 0.90−0.60 (m, 80H). ^{13}C NMR (75 MHz, $CDCl_3$, δ): 152.58, 152.12, 151.97, 148.16, 141.25, 140.71, 140.58, 140.48, 140.31, 140.22, 140.13, 140.04, 139.84, 136.17, 129.36, 126.51, 126.41, 126.32, 123.96, 122.65, 121.66, 121.57, 120.60, 120.47, 120.19, 119.59, 90.90, 55.65, 55.52, 40.71, 40.59, 31.73, 31.68, 29.95, 29.88, 24.21, 24.02, 22.85, 22.80, 14.29. MALDI-TOF m/z: 3021.6. Anal. Calcd for $C_{226}H_{276}N_2$: C 89.86, H 9.21, N 0.93. Found: C 90.17, H 9.36, N 1.05.

*1,2,3,4,5,6-Hexakis(7″-(diphenylamino)-9,9,9′,9′,9″,9″-hexahexyl-9H,9′H,9″H-2,2′:7′,2″-terfluoren-7-yl)phenyl (**HFB-diF-Dpa**).* To a mixture of **A1** (0.60 g, 0.26 mmol) and dicobaltoctacarbonyl (10 mg, 0.03 mmol) was added 60 mL of degassed 1,4-dioxane. The solution was heated to 120 °C and stirred at this temperature for 24 h under argon. After cooling to room temperature, the reaction mixture was poured into water. The solution was extracted with CH_2Cl_2, and the organic layer was dried over anhydrous Na_2SO_4. After the solvent was removed, the residue was purified by column chromatography on silica gel using petroleum ether/chloroform (10:1 by vol) as the eluent to give a yellow powder (0.40 g). Yield: 67%. ^{1}H NMR (300 MHz, $CDCl_3$, δ): 7.80−7.71 (m, 18H), 7.71−7.48 (m, 48H), 7.48−7.38 (m, 18H), 7.30−7.19 (m, 18H), 7.17−7.08 (m, 36H), 7.08−6.91 (m, 30H), 2.10−1.72 (m, 72H), 1.21−0.92 (m, 208H), 0.90−0.62 (m, 165H), 0.47−0.31 (m, 23H). ^{13}C NMR (75 MHz, $CDCl_3$, δ): 152.75, 152.55, 151.90, 151.77, 151.54, 148.13, 147.20, 140.52, 140.35, 140.26, 140.05, 139.92, 136.16, 129.34, 126.34, 126.18, 123.93, 123.76, 122.61,

Scheme 1. Synthetic Routes of HFB-diF-Dpa and HFB-terF-Dpa

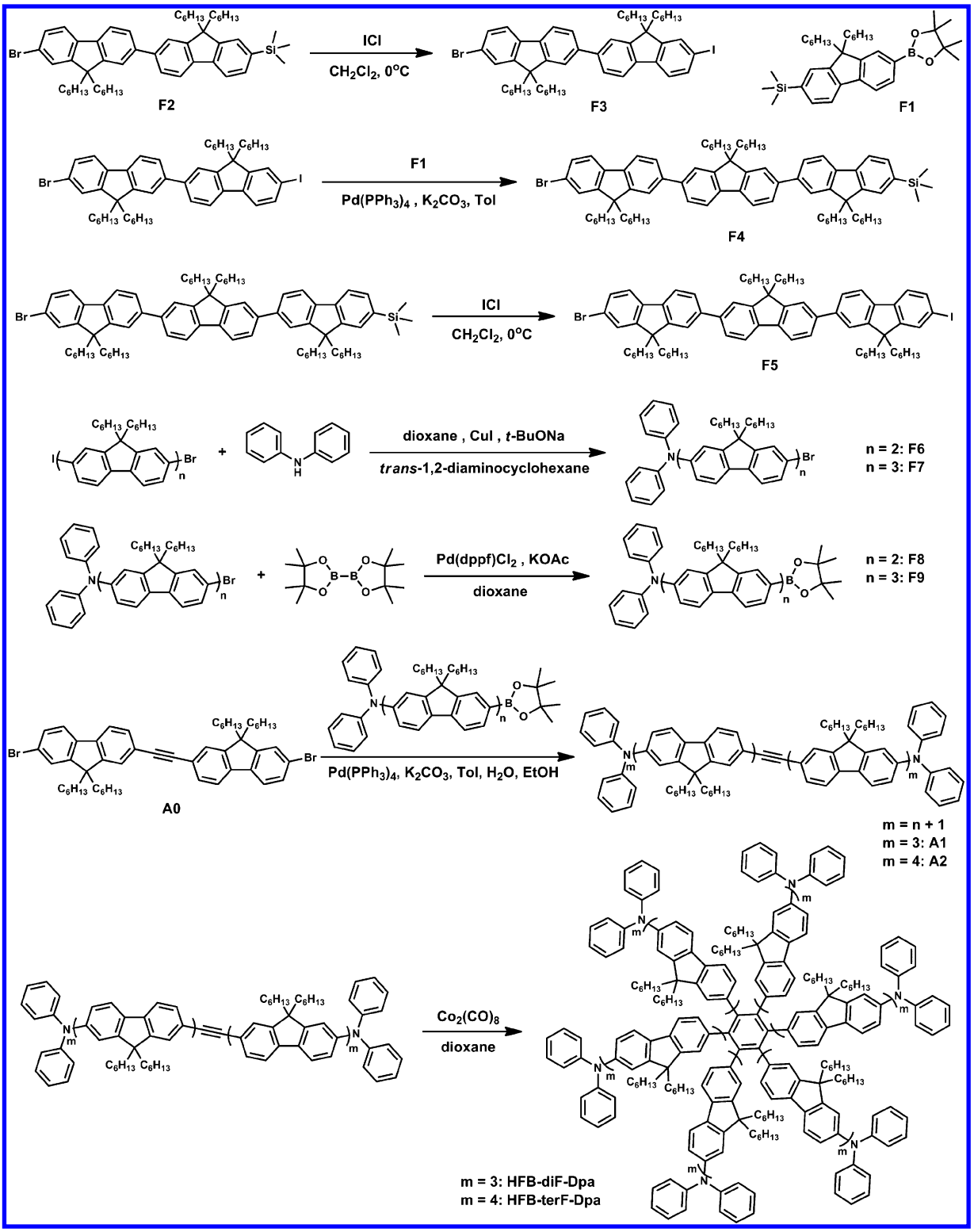

121.48, 121.36, 120.05, 119.57, 119.51, 55.36, 55.33, 54.71, 40.46, 31.77, 31.70, 31.58, 30.16, 29.81, 23.96, 23.82, 23.06, 22.76, 14.37, 14.29. MALDI-TOF *m/z*: 7066.5. Anal. Calcd for $C_{528}H_{636}N_6$: C 89.74, H 9.07, N 1.19. Found: C 89.79, H 9.40, N 1.23.

*1,2,3,4,5,6-Hexakis(7‴-(diphenylamino)-9,9,9′,9′,9″,9″,9‴,9‴-octahexy-9H,9′H,9″H,9‴H-2,2′:7′,2″:7″,2‴-quaterfluoren-7-yl)phenyl (**HFB-terF-Dpa**).* **HFB-terF-Dpa** was prepared according to the same procedure as **HFB-diF-Dpa** but using compounds **A2** to give a yellow powder. Yield: 30% .^{1}H NMR (300 MHz, $CDCl_3$, δ): 7.87−7.74 (m, 24H), 7.74−7.50 (m, 72H), 7.50−7.38 (m, 24H), 7.32−7.18 (m, 18H), 7.18−7.08 (m, 36H), 7.08−6.85 (m, 30H), 2.19−1.77 (m, 96H), 1.23−0.96 (m, 306H), 0.96−0.66 (m, 209H), 0.50−0.30 (m, 13H). ^{13}C NMR (75 MHz, $CDCl_3$, δ): 152.66, 151.91, 151.78, 148.14, 147.25, 140.61, 140.33, 140.15, 140.05, 139.89, 139.87, 136.26, 129.34, 126.24, 123.94, 122.51, 121.63, 119.43, 55.46, 55.38, 54.73, 40.51, 40.48, 31.78, 31.70, 31.64, 29.84, 23.99, 23.07, 22.77, 14.38, 14.29, 14.27. MALDI-TOF *m/z*: 9060.0. Anal. Calcd for $C_{678}H_{828}N_6$: C 89.86, H 9.21, N 0.93. Found: C 90.09, H 9.43, N 0.96.

dx.doi.org/10.1021/cm4039522 | *Chem. Mater.* 2014, 26, 3074−3083

RESULTS AND DISCUSSION

Synthesis and Characterization. The new star-shaped oligofluorenes **HFB-diF-Dpa** and **HFB-terF-Dpa** were synthesized by convergent core-creating approach as depicted in Scheme 1. The stepwise preparation of the key intermediates of alkyne derivatives **A1** and **A2** commenced with the synthesis of **F3** and **F5**, respectively, which were then subjected to the selective amination of the aryl iodide to generate **F6** and **F7** by a modified, mild Buchwald cross-coupling reaction.[50] Subsequent borylation using bis(pinacolato)diboron afforded the desired boronic acid pinacol esters **F8** and **F9**. By using Suzuki cross-coupling reactions of building block **A0** with the corresponding oligofluorene boronic acid pinacol esters (**F8** and **F9**), the alkyne derivatives of **A1** and **A2** were obtained. Finally, the target compounds **HFB-diF-Dpa** and **HFB-terF-Dpa** were successfully prepared by using dicobaltoctacarbonyl-catalyzed cyclotrimerization of **A1** and **A2**. The well-defined structures and chemical purities of all intermediates and the final star-shaped compounds were adequately verified by ^{1}H and ^{13}C NMR spectroscopy, elemental analysis, and MALDI-TOF mass spectrometry (see experimental section).

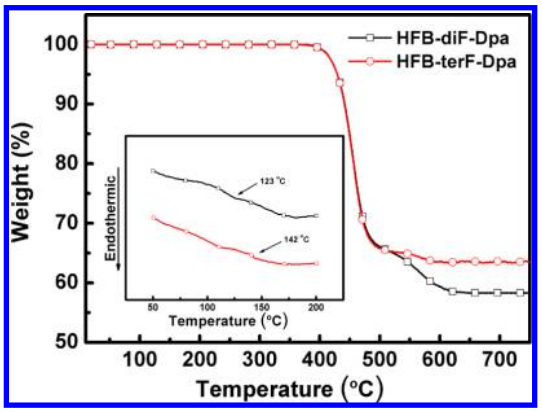

Figure 1. TGA thermograms of **HFB-diF-Dpa** and **HFB-terF-Dpa** recorded at a heating rate of 10 °C min^{-1}. Inset: DSC traces recorded at a heating rate of 10 °C min^{-1}.

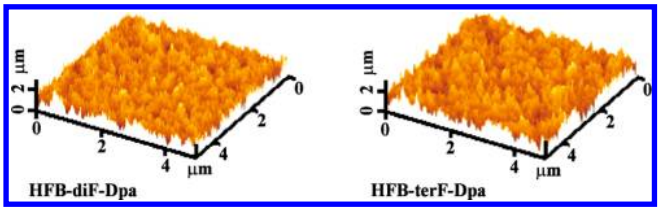

Figure 2. AFM topographic images of **HFB-diF-Dpa** and **HFB-terF-Dpa** in thin solid films.

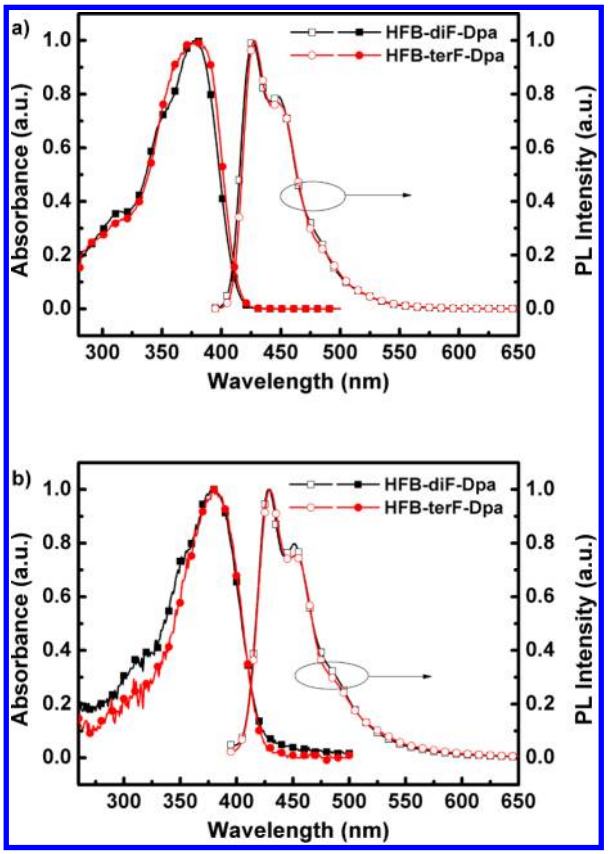

Figure 3. UV−vis absorption and PL spectra of **HFB-diF-Dpa** and **HFB-terF-Dpa** in (a) toluene solution at 5 × 10^{-6} M and (b) film state.

Thermal Properties. The good thermal stability of the compounds is indicated by their high decomposition temperatures (T_d, corresponding to 5% weight loss) of ca. 430 °C in the thermogravimetric analysis (Figure 1). Their glass transition temperatures (T_g) determined through differential scanning calorimetry are 123 °C for **HFB-diF-Dpa** and 142 °C for **HFB-terF-Dpa** (inset of Figure 1), which are significantly higher than those of the corresponding three-armed oligofluorenes based on a benzene core (T_g = 76−88 °C),[46] and poly(9,9-dihexylfluorene) (T_g = 103 °C).[51] These values are also higher than those of the six-armed oligofluorenes without diphenylamine end-capper (102 °C for T2 and 114 °C for T3) we previously reported.[42] The high T_g values can attribute to the rigid hexakis(fluoren-2-yl)benzene core and the extending molecular system.[42,52]

We also recorded atomic force microscopy (AFM) images of the compounds on ITO/PEDOT substrate to investigate their morphological stability (Figure 2). The thin film was prepared by spin-coating and then annealed under N_2 gas condition at 120 °C for 30 min. The annealed film has a fairly smooth surface morphology with a root-mean-square (rms) roughness of 0.338 for **HFB-diF-Dpa** and 0.380 nm for **HFB-terF-Dpa**. The excellent thermal and morphological stability of these materials enable the preparation of homogeneous and stable amorphous thin films through solution processing.

Photophysical Properties. Figure 3 shows the absorption and fluorescence spectra of **HFB-diF-Dpa** and **HFB-terF-Dpa** both in toluene solution and solid state films. The photophysical data of the compounds are summarized in Table 1. The absorption spectrum of each compound in toluene solution shows absorption peak around 380 nm assigned to the $\pi-\pi^*$ transition of the oligofluorenes, which reveals no red-shift in solid state film. The thin film of the two compounds display emission peaks at 429 nm and shoulder emissions at 452 nm, which only bathochromically shift 1−3 nm relative to their solution spectra, indicating the absence of intermolecular interactions in thin films. This can be attributed to the bulky star-shaped structures that have effectively restrained intermolecular aggregation. In addtion, almost the same emission peaks of the two compounds indicate that their emission tends to be saturated with sufficiently long arms. The peak emissions of **HFB-diF-Dpa** and **HFB-terF-Dpa** exhibit 12 and 20 nm

dx.doi.org/10.1021/cm4039522 | Chem. Mater. 2014, 26, 3074−3083

Table 1. Thermal, Photophysical, and Electrochemical data of HFB-diF-Dpa and HFB-terF-Dpa

compd	T_g[a] (°C)	T_d[b] (°C)	λ_{abs}[c] (nm)	λ_{abs}[d] (nm)	$\lambda_{em,max}$[c] (nm)	$\lambda_{em,max}$[d] (nm)	HOMO[e]/LUMO[f] (eV)	Φ_{PL}[g]
HFB-diF-Dpa	123	430	378	380	426, 449	429, 452	−5.10/−2.14	0.77
HFB-terF-Dpa	142	429	379	380	428, 447	429, 453	−5.10/−2.15	0.83

[a]Obtained from DSC measurements. [b]Obtained from TGA measurements. [c]Measured in toluene. [d]Measured in film. [e]Determined from the onset of oxidation potentials. [f]Deduced from HOMO and E_g estimated from the red edge of the longest absorption wavelength for the solid-film sample. [g]Fluorescence quantum yields in solid state films, measured on the quartz plate using an integrating sphere.

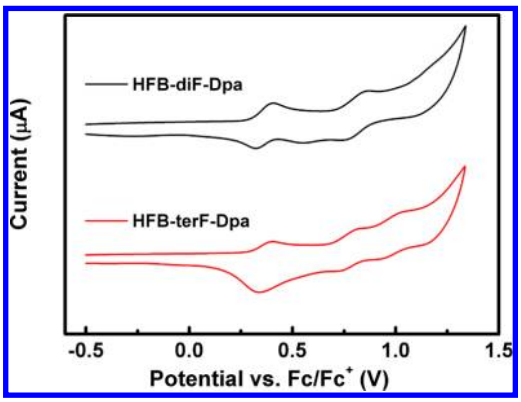

Figure 4. Cyclic voltammograms of **HFB-diF-Dpa** and **HFB-terF-Dpa** in CH_2Cl_2 for oxidation.

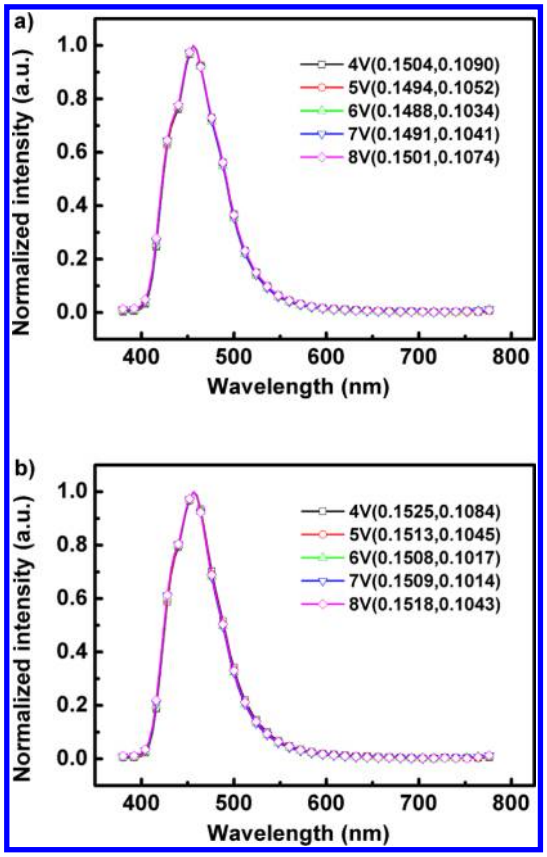

Figure 5. Normalized EL spectra of devices (a) A and (b) B recorded at various driving voltage.

redshifts in comparsion with their six-armed analogues without diphenylamine end-capper (409 nm for T2 and 417 nm for T3).[42] This suggests the excitation on the diphenylamine end groups. Fluorescence quantum yields (Φ_{PL}) of these materials in the solid state measured on the quartz plate using an integrating sphere are 0.77 for **HFB-diF-Dpa** and 0.83 for **HFB-terF-Dpa**.

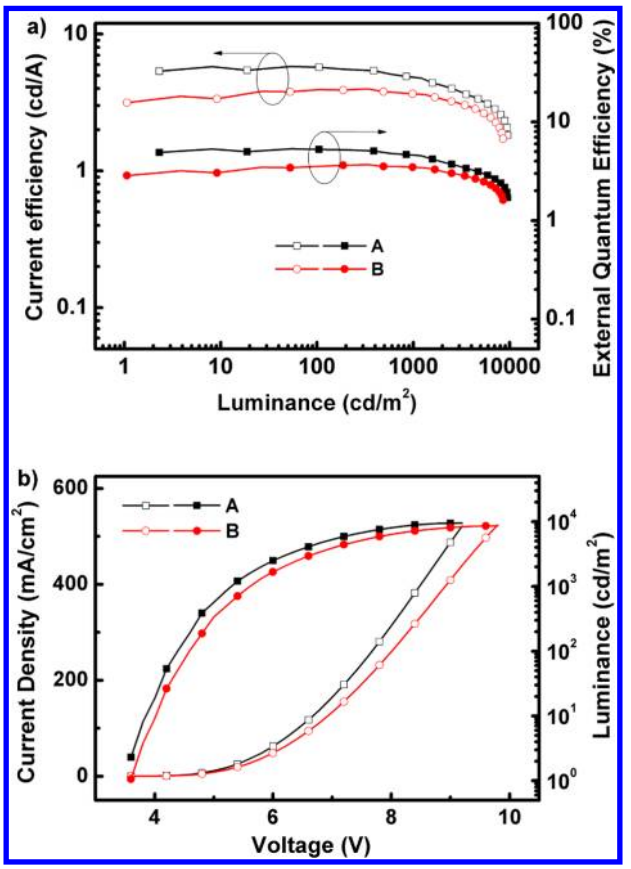

Figure 6. (a) Current efficiency and EQE versus luninance curves and (b) current density−voltage−brightness (J−V−L) characteristics for devices A and B.

Electrochemical Properties. The electrochemical behaviors of the compounds were probed by cyclic voltammetry (Figure 4). Both **HFB-diF-Dpa** and **HFB-terF-Dpa** exhibit the reversible oxidation process. The oxidation wave around 0.4 V can be attributed to the oxidation of the terminal diphenylamine groups, while oxidation waves beyond 0.5 V can be attributed to the oxidation of oligofluorene arms. **HFB-terF-Dpa** shows the second oxidation peak at 0.78 V that is slightly lower than 0.80 V of **HFB-diF-Dpa**, owing to the extended conjugation of the former. In addition, the two compounds exhibit similar oxidation peaks of oligofluorenes to their analogues without diphenylamine end-capper.[42] The highest occupied molecular orbital (HOMO) energy levels estimated from the onsets of the oxidation potentials are −5.10 eV for both the two compounds with regard to the energy level of ferrocene (4.8 eV below vacuum), which are 0.46 and 0.41 eV higher than those of their corresponding analogues without diphenylamine end-capper (5.56 eV for T2 and 5.51 eV for T3).[42] Noticeably, the HOMO levels of the two compounds

dx.doi.org/10.1021/cm4039522 | Chem. Mater. 2014, 26, 3074−3083

Table 2. Electroluminescence Characteristics of the Devices

device	emitter	HIL	V_{on}[a] (V)	L_{max}[b] (cd m^{-2}), voltage (V)	$\eta_{c,max}$[c] (cd A^{-1}), L (cd m^{-2})	$\eta_{ext,max}$[d] (%)	$\eta_{p,max}$[e] (lm W^{-1}), L (cd m^{-2})	CIE (x,y)[f]
A	**HFB-diF-Dpa**	PEDOT:PSS$_{4083}$	3.6	9524, 9.2	5.80, 53.6	5.30	4.78, 8.2	0.149, 0.104
					5.72 ± 0.08	*5.27 ± 0.04*	*4.71 ± 0.07*	
B	**HFB-terF-Dpa**	PEDOT:PSS$_{4083}$	3.6	8596, 9.8	3.97, 339.3	3.70	2.91, 3.5	0.151, 0.101
					3.91 ± 0.06	*3.64 ± 0.06*	*2.78 ± 0.13*	
C	**HFB-diF-Dpa**	PEDOT:PSS$_{8000}$	3.6	6378, 12.0	6.99, 1.5	5.45	6.10, 1.5	0.154, 0.136
					6.86 ± 0.14	*5.41 ± 0.04*	*6.02 ± 0.08*	
D	**HFB-terF-Dpa**	PEDOT:PSS$_{8000}$	3.6	6057, 11.8	6.73, 1.7	4.86	5.87, 1.7	0.154, 0.150
					6.64 ± 0.10	*4.75 ± 0.11*	*5.74 ± 0.13*	

[a]Turn-on voltage, recorded at the brightness of 1 cd m^{-2}. [b]Maximum luminance. [c]Maximum current efficiency, statistics (italic) based on 10 cells of each type. [d]Maximum external quantum efficiency, statistics (italic) based on 10 cells of each type. [e]Maximum power efficiency, statistics (italic) based on 10 cells of each type. [f]Measured at 7 V.

match well with that of the hole-injecting material poly(3,4-ethylenedioxythiopene):poly(styrenesulfonate) (PEDOT:PSS) (−5.10 eV) and would result in an efficient hole-injection from PEDOT:PSS to the emissive layer. The band gaps (E_g) of **HFB-diF-Dpa** and **HFB-terF-Dpa**, on the basis of the red edge of the longest absorption wavelength for the solid-film sample, were estimated to be 2.96 and 2.95 eV, respectively. Previous researchers had done systematical studies of the electrochemical and electronic properties for oligofluorenes. They demonstrated that the reduction behavior could not be observed in CV for oligofluorenes because a stable anionic state was not experimentally accessible.[53] In this work, we have scanned the reduction curves in THF for these multibranched oligofluorenes, and we also have not observed their electrochemical reduction behavior. Thus, the lowest unoccupied molecular orbital (LUMO) levels are deduced to be −2.15 eV by the relation LUMO = HOMO − E_g (Table 1).

Deep-Blue Electroluminescence. Both **HFB-diF-Dpa** and **HFB-terF-Dpa** exhibit deep-blue emission, high fluorescence quantum yield and good solubility in common solvents. To evaluate EL properties of these materials, simple double-layer devices, featuring the two compounds as nondoped blue emitters, were fabricated with the configurations of indium tin oxide (ITO)/PEDOT:PSS$_{4083}$ (40 nm)/emission layer (EML, 50 nm)/1,3,5-tris(*N*-phenylbenzimidazol-2-yl)-benzene (TPBI, 30 nm)/lithium fluoride (LiF, 1 nm)/aluminum (Al, 100 nm) (emitter: **HFB-diF-Dpa**, device A; **HFB-terF-Dpa**, device B), in which the emission layer was spin-coated from chlorobenzene solution. PEDOT:PSS$_{4083}$ and LiF served as hole- and electron-injecting layers, respectively. TPBI was inserted between the EML and LiF as the electron-transporting layer.

The devices based on these emitters exhibit deep-blue emission with emission maxima of 456 nm and CIE coordinates of (0.149, 0.104) for device A and (0.151, 0.101) for device B (Figure 5). The EL spectra of these materials are similar to their PL spectra in the thin film state, indicating that the formation of excimer or exciplex is effectively suppressed during the EL process. Noticeably, these devices exhibit striking blue EL color stability at various driving voltages. With increasing driving voltage from 4 to 8 V, the EL spectra of all these devices remain nearly unchanged, and the CIE coordinate values show negligible variation, suggesting a remarkable voltage-independent EL emission. The excellent color stability can be attributed to the bulky star-shaped structures that may suppress the close-packing of molecules in the solid state and then improve the morphological stability that would resist crystallization and morphological transition-induced deterioration during the device operation.

Figure 6 shows the current density−voltage−brightness (J−V−L) characteristics and efficiency versus luminance curves of the devices (Table 2). Both two devices have a low turn-on voltage of 3.6 V, which are much lower than those of their corresponding diphenylamine-absent analogues (7.8 V for T2-based device and 6.9 V for T3-based device).[42] This should be attributed to the high-lying HOMO levels of these materials, which match well with the HOMO level of adjacent PEDOT:PSS and thereby facilitate hole injection of the device. Device B exhibits good performance with a maximum current efficiency of 3.97 cd A^{-1}, a maximum power efficiency of 2.91 lm W^{-1}, and a maximum external quantum efficiency of 3.70%. Device A achieves excellent performance with a maximum luminance of 9524 cd m^{-2} at 9.2 V, a maximum current efficiency of 5.80 cd A^{-1}, a maximum power efficiency of 4.78 lm W^{-1}, and a maximum external quantum efficiency of 5.30%. The superior efficiency of devices A to B could be attributed to the following facts: (i) **HFB-diF-Dpa** possesses more smooth surface morphology (0.338 nm) than **HFB-terF-Dpa** (0.380 nm); (ii) **HFB-diF-Dpa** exhibits lower hole mobility than **HFB-terF-Dpa**, and thus, the charge flux in device A tends to be more balanced in comparison with device B. Notably, upon increasing to the practical brightness of 100 cd m^{-2}, the current and external quantum efficiency of device A are 5.73 cd A^{-1} and 5.25%, respectively, with a roll-off value of below 2%. At a high brightness of 1000 cd m^{-2}, the roll-off value of external quantum efficiency is only 12%. Even at the brightness of 5000 cd m^{-2}, the current and external quantum efficiency of device A is still above 50% of the maximum value. Although device B shows inferior performances to device A, it exhibits much lower efficiency roll-off. At a high brightness of 1000 cd m^{-2}, the roll-off values of current and external quantum efficiency are 7.8% and 6.2%, respectively.

To further improve the EL efficiency, we fabricated **HFB-diF-Dpa**-based device C and **HFB-terF-Dpa**-based device D in the same device configurations except using PEDOT:PSS$_{8000}$ with low electrical conductivity of ∼10^{-5} S cm^{-1} to replace PEDOT:PSS$_{4083}$ (∼10^{-3} S cm^{-1}). It was reported that the device with PEDOT:PSS$_{8000}$ presented more efficient attenuation of hole flux and control over electrical leakage.[54] The J−V−L characteristics and efficiency versus luminance curves are shown in Figure 7. The current densities in device C and D are lower than those of the PEDOT:PSS$_{4083}$ devices, which can be attributed to the decreased leakage current and balanced charge flux. Remarkably, the current/power efficiencies are elevated to

dx.doi.org/10.1021/cm4039522 | *Chem. Mater.* 2014, 26, 3074−3083

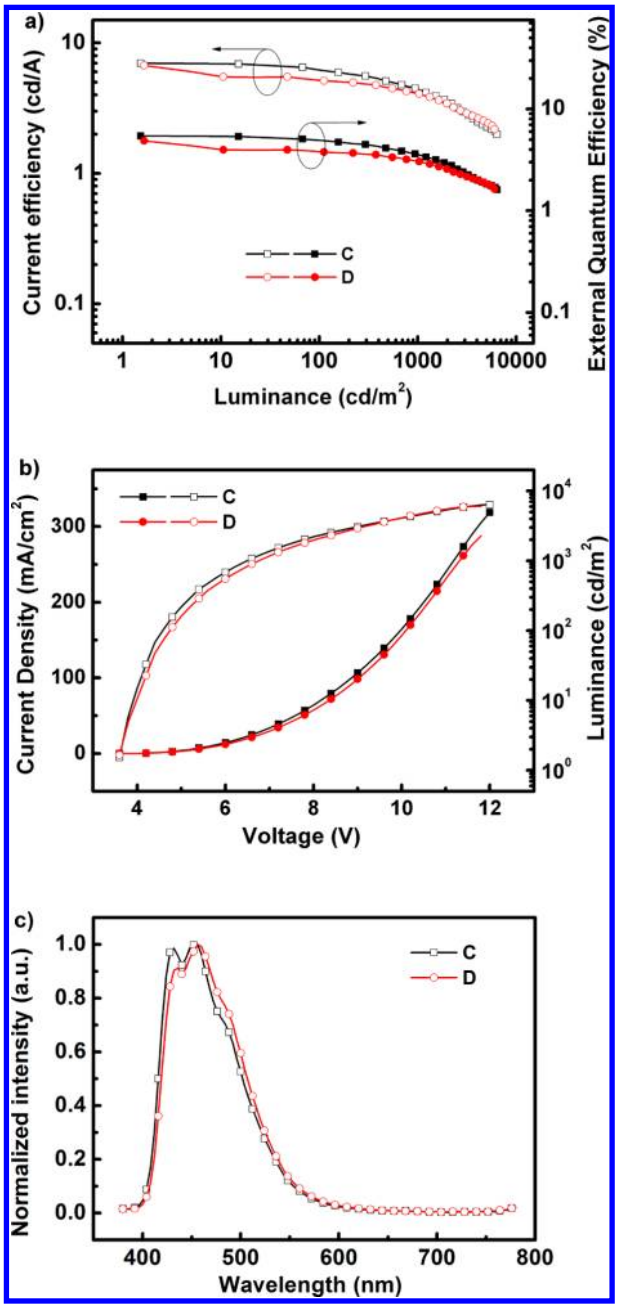

Figure 7. (a) Current efficiency and EQE versus luninance curves, (b) current density−voltage−brightness (J−V−L) characteristics, and (c) normalized EL spectra recorded at 7 V for devices C and D.

a higher level. Device C shows a maximum current efficiency of 6.99 cd A^{-1}, a maximum external quantum efficiency of 5.45%, and a maximum power efficiency of 6.10 lm W^{-1}, with the CIE coordinate of (0.154, 0.136). The **HFB-terF-Dpa**-based device D exhibits a maximum current efficiency of 6.73 cd A^{-1}, a maximum external quantum efficiency of 4.86%, and a maximum power efficiency of 5.87 lm W^{-1}, with the CIE coordinate of (0.154, 0.150). This drastic improvement could be rationalized from the fact that excess hole carriers are retarded to transport into the EML. However, because of the inferior electrical conductivity of PEDOT:PSS_{8000}, the recombination zones in devices C and D may shift toward the interface of HTL/EML, resulting in the formation of some excimers and/or exciplexes (Figure 7c). Consequently, devices C and D show a lighter blue color than devices A and B. In addition, device D exhibits more significant improvement than device C. This can be elucidated as follows: when using PEDOT:PSS_{8000} with low electrical conductivity as the hole-injecting and transporting layers, more balanced charge flux may be achieved in device D owing to the superior hole mobility of **HFB-terF-Dpa** to **HFB-diF-Dpa**. On the contrary, the charge flux in device A tends to be more balanced when using PEDOT:PSS_{4083} with relative high electrical conductivity as hole-injecting and transporting layers as we discussed before.

To the best of our knowledge, these efficiencies are among the highest for nondoped deep-blue OLEDs based on solution-processed materials.[34−42,55−65] For example, the device using TCTA-cored oligofluorenes as emitters acquired a $\eta_{c,max}$ of 0.47 cd A^{-1} and the CIE coordinates of (0.16, 0.07);[35] the device based on six-oligofluorene-arm triazatruxenes showed $\eta_{c,max}$ of 2.07 cd A^{-1} and CIE coordinates of (0.15, 0.09);[34] the device based on 1,3,5-tri(anthracen-10-yl)-benzene starburst oligofluorenes showed $\eta_{c,max}$ of 1.80 cd A^{-1} and CIE coordinates of (0.15, 0.10);[39] the device based on the star-shaped oligofluorenes with a planar triphenylamine core obtained $\eta_{c,max}$ of 3.83 cd A^{-1} and CIE coordinates of (0.15, 0.09).[40] It is noteworthy that the low driving voltage and high EQE provides an outstanding maximum power efficiency of 6.10 lm W^{-1}, which is the highest for nondoped deep-blue OLEDs based on solution-processed materials.

The unencapsulated devices can be lighted for 3 weeks in the glovebox. When the devices were exposed to the air, they remained to be emissive in 1 week, and the brightness was gradually decreased.

■ CONCLUSIONS

In summary, we have designed and synthesized two new star-shaped oligofluorenes, **HFB-diF-Dpa** and **HFB-terF-Dpa**, with a hexakis(fluoren-2-yl)benzene core and six diphenylamine end-cappers. The two compounds show excellent thermal stabilities and morphological stability, pronounced PL efficiencies, and good solution-processability. Double-layer nondoped OLEDs by solution process exhibit highly efficient and stable deep-blue electroluminescence. The **HFB-diF-Dpa**-based device achieves a maximum current efficiency of 6.99 cd A^{-1}, a maximum external quantum efficiency of 5.45%. Noticeably, the low driving voltage and high EQE result in a maximum power efficiency of 6.10 lm W^{-1}, which is the highest for nondoped deep-blue OLEDs based on solution-processed materials. Moreover, these devices present small values of efficiency roll-off at high brightness up to 1000 cd m^{-2}. Our findings provide a valuable strategy to the rational design and development of efficient blue oligofluorenes and other related materials.

■ AUTHOR INFORMATION

Corresponding Authors

*(C.Y.) E-mail: clyang@whu.edu.cn.
*(D.M.) E-mail: mdg1014@ciac.jl.cn.

Author Contributions

§(C.L. and Q.F.) These authors contributed equally to this work.

Notes

The authors declare no competing financial interest.

dx.doi.org/10.1021/cm4039522 | *Chem. Mater.* 2014, 26, 3074−3083

■ ACKNOWLEDGMENTS

We thank the National Basic Research Program of China (973 Program 2013CB834805), the National Science Fund for Distinguished Young Scholars of China (No.51125013), and the Research Fund for the Doctoral Program of Higher Education of China (20120141110029) for financial support.

■ REFERENCES

(1) D'Andrade, B. W.; Forrest, S. R. *Adv. Mater.* **2004**, *16*, 1585.
(2) Baldo, M. A.; Thompson, M. E.; Forrest, S. R. *Nature* **2000**, *403*, 750.
(3) Burroughes, J. H.; Bradley, D. D. C.; Brown, A. R.; Marks, R. N.; Mackay, K.; Friend, R. H.; Burn, P. L.; Holmes, A. B. *Nature* **1990**, *347*, 539.
(4) Chien, C. H.; Chen, C. K.; Hsu, F. M.; Shu, C. F.; Chou, P. T.; Lai, C. H. *Adv. Funct. Mater.* **2009**, *19*, 560.
(5) Zhang, M.; Xue, S.; Dong, W.; Wang, Q.; Fei, T.; Gu, C.; Ma, Y. *Chem. Commun.* **2010**, *46*, 3923.
(6) Jiang, Z.; Liu, Z.; Yang, C.; Zhong, C.; Qin, J.; Yu, G.; Liu, Y. *Adv. Funct. Mater.* **2009**, *19*, 3987.
(7) Gong, S.; Zhao, Y.; Wang, M.; Yang, C.; Zhong, C.; Qin, J.; Ma, D. *Chem.—Asian J.* **2010**, *5*, 2093.
(8) Zhu, M.; Wang, Q.; Gu, Y.; Cao, X.; Zhong, C.; Ma, D.; Qin, J.; Yang, C. *J. Mater. Chem.* **2011**, *21*, 6409.
(9) Zhu, M.; Ye, T.; Li, C.-G.; Cao, X.; Zhong, C.; Ma, D.; Qin, J.; Yang, C. *J. Phys. Chem. C* **2011**, *115*, 17965.
(10) Gong, S.; Yang, C.; Qin, J. *Chem. Soc. Rev.* **2012**, *41*, 4797.
(11) Liu, C.; Gu, Y.; Fu, Q.; Sun, N.; Zhong, C.; Ma, D.; Qin, J.; Yang, C. *Chem.—Eur. J.* **2012**, *18*, 13828.
(12) Grimsdale, A. C.; Leok Chan, K.; Martin, R. E.; Jokisz, P. G.; Holmes, A. B. *Chem. Rev.* **2009**, *109*, 897.
(13) Zhu, M.; Yang, C. *Chem. Soc. Rev.* **2013**, *42*, 4963.
(14) Lee, M. *Appl. Phys. Lett.* **2004**, *85*, 3301.
(15) Lee, M. T.; Liao, C. H.; Tsai, C. H.; Chen, C. H. *Adv. Mater.* **2005**, *17*, 2493.
(16) Lee, S. J.; Park, J. S.; Yoon, K.-J.; Kim, Y.-I.; Jin, S.-H.; Kang, S. K.; Gal, Y.-S.; Kang, S.; Lee, J. Y.; Kang, J.-W.; Lee, S.-H.; Park, H.-D.; Kim, J.-J. *Adv. Funct. Mater.* **2008**, *18*, 3922.
(17) Saragi, T. P.; Spehr, T.; Siebert, A.; Fuhrmann-Lieker, T.; Salbeck, J. *Chem. Rev.* **2007**, *107*, 1011.
(18) Fisher, A. L.; Linton, K. E.; Kamtekar, K. T.; Pearson, C.; Bryce, M. R.; Petty, M. C. *Chem. Mater.* **2011**, *23*, 1640.
(19) Grimsdale, A. C.; Müllen, K. *Macromol. Rapid Commun.* **2007**, *28*, 1676.
(20) Grice, A.; Bradley, D.; Bernius, M.; Inbasekaran, M.; Wu, W.; Woo, E. *Appl. Phys. Lett.* **1998**, *73*, 629.
(21) Kreyenschmidt, M.; Klaerner, G.; Fuhrer, T.; Ashenhurst, J.; Karg, S.; Chen, W.; Lee, V.; Scott, J.; Miller, R. *Macromolecules* **1998**, *31*, 1099.
(22) Kannan, R.; He, G. S.; Yuan, L.; Xu, F.; Prasad, P. N.; Dombroskie, A. G.; Reinhardt, B. A.; Baur, J. W.; Vaia, R. A.; Tan, L.-S. *Chem. Mater.* **2001**, *13*, 1896.
(23) Hung, M.-C.; Liao, J.-L.; Chen, S.-A.; Chen, S.-H.; Su, A.-C. *J. Am. Chem. Soc.* **2005**, *127*, 14576.
(24) Huang, F.; Zhang, Y.; Liu, M. S.; Cheng, Y. J.; Jen, A. Y. *Adv. Funct. Mater.* **2007**, *17*, 3808.
(25) Zhao, Q.; Liu, S. J.; Huang, W. *Macromol. Chem. Phys.* **2009**, *210*, 1580.
(26) Huber, J.; Müllen, K.; Salbeck, J.; Schenk, H.; Scherf, U.; Stehlin, T.; Stern, R. *Acta Polym.* **1994**, *45*, 244.
(27) Jenekhe, S. A.; Osaheni, J. A. *Science* **1994**, *265*, 765.
(28) Lemmer, U.; Heun, S.; Mahrt, R. F.; Scherf, U.; Hopmeier, M.; Siegner, U.; Göbel, E. O.; Müllen, K.; Bässler, H. *Chem. Phys. Lett.* **1995**, *240*, 373.
(29) Chan, K. L.; Sims, M.; Pascu, S. I.; Ariu, M.; Holmes, A. B.; Bradley, D. D. C. *Adv. Funct. Mater.* **2009**, *19*, 2147.
(30) Poriel, C.; Cocherel, N.; Rault-Berthelot, J.; Vignau, L.; Jeannin, O. *Chem.—Eur. J.* **2011**, *17*, 12631.
(31) List, E. J.; Guentner, R.; Scanducci de Freitas, P.; Scherf, U. *Adv. Mater.* **2002**, *14*, 374.
(32) Cho, S. Y.; Grimsdale, A. C.; Jones, D. J.; Watkins, S. E.; Holmes, A. B. *J. Am. Chem. Soc.* **2007**, *129*, 11910.
(33) Katsis, D.; Geng, Y. H.; Ou, J. J.; Culligan, S. W.; Trajkovska, A.; Chen, S. H.; Rothberg, L. J. *Chem. Mater.* **2002**, *14*, 1332.
(34) Lai, W.-Y.; Zhu, R.; Fan, Q.-L.; Hou, L.-T.; Cao, Y.; Huang, W. *Macromolecules* **2006**, *39*, 3707.
(35) Liu, Q. D.; Lu, J.; Ding, J.; Day, M.; Tao, Y.; Barrios, P.; Stupak, J.; Chan, K.; Li, J.; Chi, Y. *Adv. Funct. Mater.* **2007**, *17*, 1028.
(36) Lai, W. Y.; He, Q. Y.; Zhu, R.; Chen, Q. Q.; Huang, W. *Adv. Funct. Mater.* **2008**, *18*, 265.
(37) Liu, F.; Lai, W.-Y.; Tang, C.; Wu, H.-B.; Chen, Q.-Q.; Peng, B.; Wei, W.; Huang, W.; Cao, Y. *Macromol. Rapid Commun.* **2008**, *29*, 659.
(38) Kanibolotsky, A. L.; Perepichka, I. F.; Skabara, P. J. *Chem. Soc. Rev.* **2010**, *39*, 2695.
(39) Huang, H.; Fu, Q.; Zhuang, S.; Liu, Y.; Wang, L.; Chen, J.; Ma, D.; Yang, C. *J. Phys. Chem. C* **2011**, *115*, 4872.
(40) Liu, C.; Li, Y.; Zhang, Y.; Yang, C.; Wu, H.; Qin, J.; Cao, Y. *Chem.—Eur. J.* **2012**, *18*, 6928.
(41) Liu, C.; Li, Y.; Li, Y.; Yang, C.; Wu, H.; Qin, J.; Cao, Y. *Chem. Mater.* **2013**, *25*, 3320.
(42) Zou, Y.; Zou, J.; Ye, T.; Li, H.; Yang, C.; Wu, H.; Ma, D.; Qin, J.; Cao, Y. *Adv. Funct. Mater.* **2013**, *23*, 1781.
(43) Gaal, M.; List, E. J.; Scherf, U. *Macromolecules* **2003**, *36*, 4236.
(44) Geng, Y.; Culligan, S. W.; Trajkovska, A.; Wallace, J. U.; Chen, S. H. *Chem. Mater.* **2003**, *15*, 542.
(45) Gong, X.; Iyer, P. K.; Moses, D.; Bazan, G. C.; Heeger, A. J.; Xiao, S. S. *Adv. Funct. Mater.* **2003**, *13*, 325.
(46) Zhou, X.-H.; Yan, J.-C.; Pei, J. *Org. Lett.* **2003**, *5*, 3543.
(47) Kanibolotsky, A. L.; Berridge, R.; Skabara, P. J.; Perepichka, I. F.; Bradley, D. D. C.; Koeberg, M. *J. Am. Chem. Soc.* **2004**, *126*, 13695.
(48) Forrest, S. R.; Bradley, D. D. C.; Thompson, M. E. *Adv. Mater.* **2003**, *15*, 1043.
(49) Dudek, S. P.; Pouderoijen, M.; Abbel, R.; Schenning, A. P. H. J.; Meijer, E. W. *J. Am. Chem. Soc.* **2005**, *127*, 11763.
(50) Klapars, A.; Antilla, J. C.; Huang, X.; Buchwald, S. L. *J. Am. Chem. Soc.* **2001**, *123*, 7727.
(51) Liu, B.; Yu, W.-L.; Lai, Y.-H.; Huang, W. *Chem. Mater.* **2001**, *13*, 1984.
(52) Zou, Y.; Ye, T.; Ma, D.; Qin, J.; Yang, C. *J. Mater. Chem.* **2012**, *22*, 23485.
(53) Chi, C.; Wegner, G. *Macromol. Rapid Commun.* **2005**, *26*, 1532.
(54) Wu, H.; Zou, J.; An, D.; Liu, F.; Yang, W.; Peng, J.; Mikhailovsky, A.; Bazan, G. C.; Cao, Y. *Org. Electron.* **2009**, *10*, 1562.
(55) Zhao, L.; Li, C.; Zhang, Y.; Zhu, X.-H.; Peng, J.; Cao, Y. *Macromol. Rapid Commun.* **2006**, *27*, 914.
(56) Luo, J.; Zhou, Y.; Niu, Z.-Q.; Zhou, Q.-F.; Ma, Y.; Pei, J. *J. Am. Chem. Soc.* **2007**, *129*, 11314.
(57) Tonzola, C. J.; Kulkarni, A. P.; Gifford, A. P.; Kaminsky, W.; Jenekhe, S. A. *Adv. Funct. Mater.* **2007**, *17*, 863.
(58) Lee, T.-W.; Noh, T.; Shin, H.-W.; Kwon, O.; Park, J.-J.; Choi, B.-K.; Kim, M.-S.; Shin, D. W.; Kim, Y.-R. *Adv. Funct. Mater.* **2009**, *19*, 1625.
(59) Wang, L.; Jiang, Y.; Luo, J.; Zhou, Y.; Zhou, J.; Wang, J.; Pei, J.; Cao, Y. *Adv. Mater.* **2009**, *21*, 4854.
(60) Zhen, C.-G.; Chen, Z.-K.; Liu, Q.-D.; Dai, Y.-F.; Shin, R. Y. C.; Chang, S.-Y.; Kieffer, J. *Adv. Mater.* **2009**, *21*, 2425.
(61) Duan, L.; Hou, L.; Lee, T.-W.; Qiao, J.; Zhang, D.; Dong, G.; Wang, L.; Qiu, Y. *J. Mater. Chem.* **2010**, *20*, 6392.
(62) Qin, T.; Wiedemair, W.; Nau, S.; Trattnig, R.; Sax, S.; Winkler, S.; Vollmer, A.; Koch, N.; Baumgarten, M.; List, E. J.; Mullen, K. *J. Am. Chem. Soc.* **2011**, *133*, 1301.
(63) Zhen, C.-G.; Dai, Y.-F.; Zeng, W.-J.; Ma, Z.; Chen, Z.-K.; Kieffer, J. *Adv. Funct. Mater.* **2011**, *21*, 699.
(64) Lo, S.-C.; Harding, R. E.; Shipley, C. P.; Stevenson, S. G.; Burn, P. L.; Samuel, I. D. W. *J. Am. Chem. Soc.* **2009**, *131*, 16681.

(65) Macdonald, J.; O'Connell, J.; Weber, K.; Hirai, T.; Groarke, M.; Andresen, S.; Bown, M.; Ueno, K. *SID Symp. Dig. Tech. Pap.* **2012**, *43*, 445.